Technobius Physics, 2024, 2(1), 0007, DOI: https://doi.org/10.54355/tbusphys/2.1.2024.0007

Technobius Physics

https://technobiusphysics.kz/

e-ISSN
3007-0147

Corrigendum Notice: A corrigendum has been issued for this article and is included at the end of this document.

Article

Comparative analysis of copper X-radiation intensity with LiF and KBr crystals

Dias Sagatov*

Laboratory of Energy Storage Systems, National Laboratory Astana, 53 Kabanbay ave., Astana, Kazakhstan
*Correspondence: dias.sagatov@list.ru

Abstract. The intensity of copper X-radiation has been scrutinized as a function of the Bragg angle, employing both LiF and KBr crystals. X-ray intensity spectra were recorded for Cu as a function of Bragg angle using LiF, KBr single crystals using a PHYWE X-Ray Expert Unit (35 kV, 1 mA) with an X-ray goniometer, Plug-in Cu X-ray tube and a 2.2 mm diameter aperture tube. The scanning range was chosen to be 4°-55° for LiF and 3°-75° for KBr. The resultant spectra furnish a comprehensive portrayal of the variation in X-ray emission intensity relative to alterations in the Bragg angle. This investigation contributes to our comprehension of crystallographic phenomena and underscores the efficacy of diverse crystalline materials in X-ray diffraction studies. Precise determinations of the energy levels for characteristic copper X-ray lines have been obtained, revealing E $(K\beta)$ = 8868.374 ± 30.474 eV and $(K\alpha)$ = 8026.349 ± 31.634 eV. These findings accentuate the significance of X-ray spectroscopy in delineating the elemental composition and structural attributes of materials, while also affirming the role of theoretical predictions in elucidating experimental observations.
Keywords: X-ray spectroscopy, Bragg angle, copper X-radiation, crystallographic phenomena, energy determination.

1. Introduction

Undoubtedly, X-ray diffraction stands as the cornerstone of solid-state physics and chemistry, representing the most pivotal and extensively utilized technique within these fields. X-ray generation stemming from collisions between protons or light ions and atoms stands as a pivotal area of investigation for understanding inner-shell ionization mechanisms. This subject has undergone extensive examination from experimental and theoretical standpoints over recent decades, yielding significant insights. Notably, extensive collections of experimental X-ray cross-section data have been assembled for K and L shells ionized by protons and helium ions, enabling meticulous comparisons with established theoretical models [1–5].

When high-energy electrons collide with the metallic anode within an X-ray tube, they generate X-rays characterized by a continuous energy spectrum. Embedded within this continuum are specific X-ray lines, known as characteristic X-ray lines, which remain independent of the anode voltage and are unique to the composition of the anode material. These lines originate from the ionization of an anode atom's K shell when struck by an electron. Subsequently, the resulting vacancy within the shell is filled by an electron transitioning from a higher energy level. The energy liberated during this de-excitation process manifests as an X-ray emission distinct to the anode atom.

X-ray spectroscopy serves as a pivotal tool in the realm of material characterization, offering unparalleled insights into the elemental composition and structural properties of diverse substances. The analysis of X-ray emission intensity as a function of the Bragg angle, facilitated by crystals such as LiF and KBr, constitutes a fundamental aspect of X-ray diffraction studies [6–8]. This investigation aims to elucidate the intricate relationship between Bragg angle variations and copper X-radiation intensity, thereby advancing our understanding of crystallographic phenomena. Additionally, precise determinations of energy levels for characteristic copper X-ray lines further underscore the utility of X-ray spectroscopy in unraveling the intricacies of material properties. By combining experimental observations with theoretical predictions, this study endeavors to provide a comprehensive framework for interpreting X-ray diffraction data and exploring the structural characteristics of materials at the atomic level [9-10].

The aim of this article is to explore and elucidate the phenomenon of X-ray production resulting from collisions between protons or other light ions and atoms. By examining this process from both experimental and theoretical perspectives, the article seeks to enhance our understanding of inner-shell ionization mechanisms. Additionally, it aims to provide detailed comparisons between experimental X-ray cross-section data and existing theoretical models, thereby advancing the current understanding of X-ray generation in such collisions.

2. Methods

X-ray diffraction spectra were collected using mounted single crystals of lithium fluoride (LiF) and potassium bromide (KBr), both with crystallographic orientation (100). Each crystal had a thickness of 1 mm and a usable surface area of 10 × 12 mm. The LiF crystals were polished, while the KBr crystals remained unpolished. Crystals were sourced from Crystal GmbH (Germany) and assumed to be free of impurities. The known lattice spacings were 201.4 pm for LiF and 329 pm for KBr.

Measurements were performed using the HUBER X-ray Diffraction System, configured with the Copper Anode X-ray Tube (40 kV, 1 mA); Primary Beam Collimator (2.2 mm aperture); High-Precision Goniometer (HUBER 420); Geiger-Müller Detector (15 mm window, Ludlum or equivalent). A schematic of the experimental setup is shown in Figure 1.

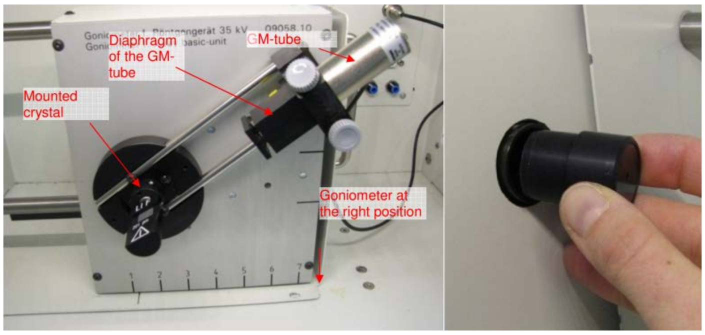

Figure 1 – Installation of X-ray goniometer and Geiger-Muller counter tube

The copper anode generated characteristic X-rays, which were directed onto the LiF or KBr crystal. The resulting diffracted beams were detected at various Bragg angles using the Geiger-Müller counter.

Intensity spectra were recorded as a function of the Bragg angle (θ) by rotating the goniometer-controlled crystal-detector stage. Scan parameters were for angular range: 4°–55° for LiF and 3°–75° for KBr; angle step width: 0.1°; gate time: 2 s per point. All scanning procedures and data acquisition were performed using SPEC Control Software (Certified Scientific Software, USA). The goniometer system was calibrated using internal standards and factory-aligned optics. All experiments were carried out under ambient laboratory conditions without additional vacuum or environmental control.

The X-ray intensity spectra have been recorded for copper as a function of Bragg angle using mounted LiF, KBr single crystals. Crystals were sourced from Crystal GmbH (Germany) and assumed to be free of impurities. X-ray spectra were recorded using a PHYWE X-Ray Expert Unit (35 kV, 1mA) with X-ray goniometer, X-ray Plug-in Cu tube and Diaphragm tube with the diameter of 2.2 mm (Figure 1). An X-ray tube with a copper anode generates X-radiation that is selected with the aid of a mounted crystal (LiF and KBr) as a function of the Bragg angle. A Geiger-Muller counter tube with the size of 15 mm measures the intensity of the radiation. The glancing angles of the characteristic X-ray lines are then used to determine the energy. The spectra were scanned in the range 4°-55° for LiF and 3°-75° for KBr with the gate time of 2 s and angle step width 0.1° using a XR 4.0 Software. The goniometer has been programmed for automatic calibration to obtain accurate reflection angles.

The Bragg angles (θ) obtained from the recorded intensity spectra were used to calculate the corresponding X-ray wavelengths (λ) and photon energies (E) using Bragg's law and the energy-wavelength relation:

$$\lambda = \frac{2d\sin\theta}{n} \text{ and } E = \frac{hc}{\lambda} \quad (1)$$

where *d* is the interplanar spacing, *h* is Planck's constant (6.626×10^{-34} J·s), ccc is the speed of light (3.00×10^{8} m/s), and n=1 for first-order diffraction. Energies were expressed in electronvolts (eV).

To ensure reliability, each peak angle was measured in triplicate, and the mean and standard deviation (SD) of the measured angles were calculated. Propagation of error was applied to determine uncertainty in the calculated wavelengths and energies:

$$\sigma_E = \frac{dE}{d\theta} \cdot \sigma_\theta \quad (2)$$

σ_θ is the standard deviation of the angle measurements.

All statistical analyses, including mean, SD, and propagation of error, were performed using OriginPro 2020 (OriginLab Corporation, USA). Graphical representations of the spectra and energy distributions were also generated in OriginPro. Results were considered statistically reliable if relative uncertainties in peak energy were below 2%.

3. Results and Discussion

As is known, when high-energy electrons hit the metal anode of an X-ray tube, X-rays with a continuum energy distribution are produced. We have analyzed polychromatic X-rays using LiF and KBr crystals (Figure 2–3).

Figure 2 presents copper X-ray intensity specrtra recorded in range of 4°-55° for LiF crystals. The curve has a distinct peaks overlaying the continuous spectrum of the bremsstrahlung. The positions of these peaks remain consistent regardless of fluctuations in the anode voltage, suggesting their characteristic nature as copper lines. The initial set of lines corresponds to the first order of diffraction (n = 1), whereas the subsequent set corresponds to n = 2. This arises from the condition where X-rays of wavelength λ approach the crystal at an angle v, leading to constructive interference post-scattering only when the path difference δ between the partial waves reflected from the lattice planes equals one or more wavelengths.

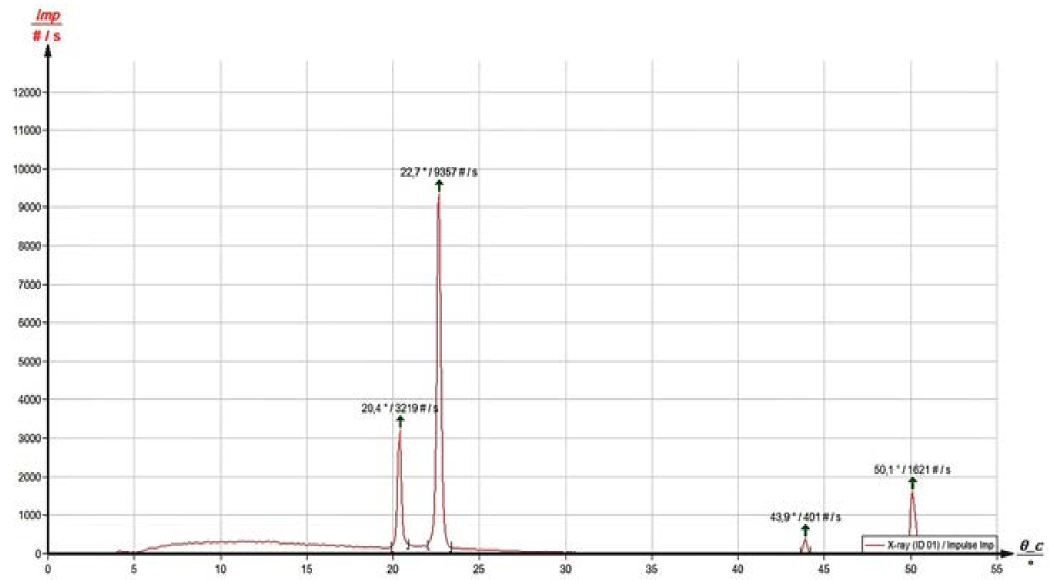

Figure 2 – Copper X-ray intensity as a function of the angle of incidence with LiF crystal as a Bragg analyzer

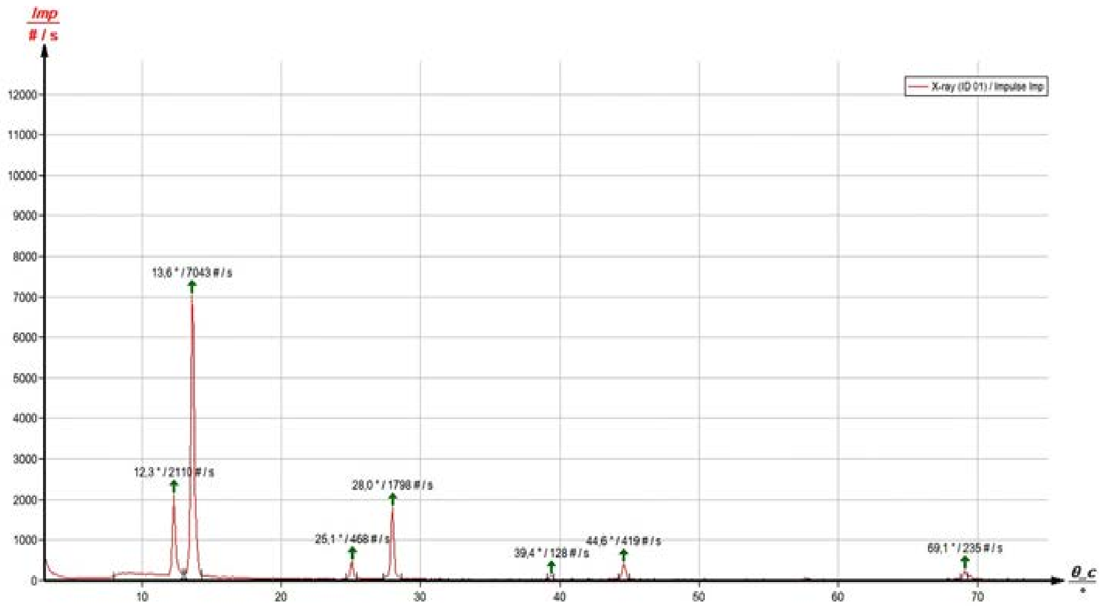

Figure 3 – Copper X-ray intensity as a function of the angle of incidence with KBr crystal as a Bragg analyzer

Substituting the LiF crystal with a KBr crystal in the examination of the copper X-ray spectrum permits Bragg scatterings up to the fourth order of diffraction (n = 4) as illustrated in Figure 3. The supplementary patterns observed beyond those depicted in Figure 3 stem from the increased lattice constant of the KBr crystal. The maximums recorded during X-ray irradiation in range of 3°-75° also refer to characteristic copper peaks.

The bremsstrahlung spectrum depicted in Figure 3 exhibits a significant decrease in intensity towards smaller angles, notably at 8.0° and 16.3°. This decline aligns precisely with the theoretically anticipated bromide K absorption edge (E_K = 13.474 keV) within the first and second orders of diffraction. However, the potassium, lithium, and fluorine K absorption edges remain undetectable due to the bremsstrahlung spectrum's insufficient intensity within these energy ranges.

The experimentally obtained values for the diffraction angles and their corresponding energies are summarized in Table 1 and Table 2.

Table 1 – Obtained experimental data of alkali halide crystals

Crystals	Initiation, deg	Maximum, deg	Shift, deg	Height, no/s	Area, no/s^2
LiF	19.8	20.5	20.8	3220.0	1022.0
	22.1	22.8	23.2	9355.1	3123.4
	43.7	44.0	44.1	405.11	102.5
	49.7	50.2	50.5	1624.2	567.8
KBr	8.0	12.4	12.8	2110.3	1302.1
	13.2	13.3	14.2	7043.4	2209.2
	24.9	25.2	25.2	468.12	141.25
	27.2	28.1	28.4	1798.3	554.62
	39.3	39.5	39.3	128.21	39.83
	44.1	44.7	45.1	419.01	149.14
	68.6	69.2	69.2	235.31	71.23

For both LiF and KBr crystals, the calculated energy values of Kα and Kβ lines align closely with the expected energy transitions for copper: approximately 8.0 keV for Kα and 8.8 keV for Kβ. Slight variations between crystals and diffraction orders are attributed to measurement uncertainties and angular resolution limits, as well as the influence of surface treatment differences—LiF being polished, while KBr was used untreated.

Table 2 – The calculated energy values pertaining to the characteristic copper X-ray lines

Crystals	Level	υ/°, deg	Line	E_{exp}, keV
LiF	n = 1	20.3	K_β	8831.201
		22.6	K_α	7975.936
	n = 2	43.8	K_β	8877.862
		50.2	K_α	8024.243
KBr	n = 1	12.2	K_β	8844.761
		13.7	K_α	8013.031
	n = 2	25.2	K_β	8883.512
		28.1	K_α	8025.795
	n = 3	39.5	K_β	8904.498
		44.7	K_α	8051.154
	n = 4		K_β	
		69.3	K_α	8067.587

The ability to resolve up to fourth-order diffractions using KBr highlights its utility for high-resolution spectral analysis. Moreover, the consistent appearance of characteristic energies across multiple orders and crystals supports the reproducibility of the experimental approach. The data obtained not only confirm the fundamental principles of X-ray diffraction but also demonstrate the comparative advantages of different crystal analyzers in resolving spectral details.

4. Conclusions

The intensity of copper X-radiation has been analyzed as a function of the Bragg angle, utilizing both LiF and KBr crystals. The observed spectra offer a comprehensive depiction of how the intensity of X-ray emissions varies with changes in the Bragg angle, thereby contributing to our understanding of crystallographic phenomena and the utility of different crystalline materials in X-ray diffraction studies.

Furthermore, the calculated energy values for the characteristic copper X-ray lines yield E ($K\beta$) = 8868.374 ± 30.474 eV and ($K\alpha$) = 8026.349 ± 31.634 eV, providing precise determinations for these energy levels. These findings underscore the utility of X-ray spectroscopy in elucidating the elemental composition and structural characteristics of materials, while also highlighting the efficacy of theoretical predictions in interpreting experimental observations.

References

1. Empirical K-shell ionization cross-sections of elements from 4Be to 92U by proton impact / A. Kahoul, M. Nekkab, B. Deghfel // Nuclear Instruments and Methods in Physics Research, Section B: Beam Interactions with Materials and Atoms. — 2008. — Vol. 266, No. 23. — P. 4969–4975. https://doi.org/10.1016/j.nimb.2008.09.008
2. Feasibility study of thin films deposited on a self-supporting carbon grid substrate target on the measurement of atomic inner-shell ionization cross-sections impacted by 3-30 keV electrons / Z. C. Qian, Y. Wu, C. H. Chang, Y. Yuan, C. S. Mei, J. J. Zhu, K. Moharram // EPL. — 2017. — Vol. 118, No. 1. — Article number. 13001. https://doi.org/10.1209/0295-5075/118/13001
3. Present status of the experimental L-shell ionization cross sections for light ion impact / I. Orlic // Nuclear Instruments and Methods in Physics Research Section B: Beam Interactions with Materials and Atoms. — 1994. — Vol. 87, No. 1. — P. 285–292. https://doi.org/10.1016/0168-583X(94)95274-4
4. Theoretical models to calculate stopping and ionization ratios of H2+ molecules in solid targets / C. D. Archubi, N. R. N. Arista // Physical Review A. — 2019. — Vol. 99, No. 3. — Article number 032702. https://doi.org/10.1103/PhysRevA.99.032702
5. Cooper-minimum-type structure in proton-induced L1- and L3- subshell x-ray line intensities of Pd measured with high-resolution x-ray spectroscopy / M. Kavčič, Ž. Šmit // Physical Review A. — 2009. — Vol. 79, No. 5. — P. 052708. https://doi.org/10.1103/PhysRevA.79.052708
6. Phase Assemblage of the Li+,Na+,K+||F–,Cl–,Br– Five-Component Reciprocal System and Its LiF–KCl–KBr–NaBr–NaCl Stable Pentatope / A.V. Burchakov, I. K. Garkushin, U. A. Emel'yanova Russian Journal of Inorganic Chemistry. — 2023. — Vol. 68, No. 7. — P.889–897. https://doi.org/10.1134/S003602362360082X

7. 3D Atomic Arrangement at Functional Interfaces Inside Nanoparticles by Resonant High-Energy X-ray Diffraction / V. Petkov, B. Prasai, S. Shastri, T.-Y. Chen // ACS Applied Materials and Interfaces. — 2015. — Vol. 7, No. 41. — P. 23265–23277. https://doi.org/10.1021/acsami.5b07391
8. Measurement of Fall Rate and Analysis of Atmospheric Falling Dust in Duhok Governorate of Iraq by Using Atomic Absorption Spectrometry and X-ray Diffraction / B.H. Mahdi // Journal of Physics: Conference Series. — 2021. — Vol. 1829. — P. 012001. https://doi.org/10.1088/1742-6596/1829/1/012001
9. Inhomogeneous thermal expansion of metallic glasses in atomic-scale studied by in-situ synchrotron X-ray diffraction / A.H. Taghvaei, H. Shakur Shahabi, J. Bednarčik, J. Eckert // Journal of Applied Physics. — 2015. — Vol. 117, No. 4. — P. 187–195. https://doi.org/10.1063/1.4906552
10. Study of the structural quality of heteroepitaxial silicon-on-sapphire structures by high-resolution X-ray diffraction, X-ray reflectivity, and electron microscopy / A.E. Blagov, A.L. Vasiliev, A.S. Golubeva, I.A. Ivanov, O.A. Kondratev, Yu.V. Pisarevsky, M.Yu. Presnyakov, P.A. Prosekov, A.Yu. Seregin // Crystallography Reports. — 2014. — Vol. 59, No. 3. — P. 315–322. https://doi.org/10.1134/S1063774514030043

Information about author:

Dias Sagatov – Research Assistant, Laboratory of Energy Storage Systems, National Laboratory Astana, 53 Kabanbay ave., Astana, Kazakhstan, dias.sagatov@list.ru

Author Contributions:

Dias Sagatov – concept, methodology, resources, data collection, testing, modeling, analysis, visualization, interpretation, drafting, editing, funding acquisition.

Conflict of Interest: The authors declare no conflict of interest.

Use of Artificial Intelligence (AI): The authors declare that AI was not used.

Received: 03.10.2023
Revised: 23.10.2023
Accepted: 13.11.2023
Published: 16.01.2024

Technobius Physics, 2024, 2(1), 0007c, DOI: https://doi.org/10.54355/tbusphys/2.1.2024.0007c

Technobius Physics

https://technobiusphysics.kz/

e-ISSN

3007-0147

Corrigendum Notice: A corrigendum has been issued for this article and is included at the end of this document.

Post-Publication Notice

Corrigendum to "D. Sagatov, "Comparative analysis of copper X-radiation intensity with LiF and KBr crystals", tbusphys, vol. 2, no. 1, p. 0007, Jan. 2024. doi: 10.54355/tbusphys/2.1.2024.0007"

In the originally published version of this article, the Methods section lacked detailed information about the experimental apparatus specifications, data acquisition process, and statistical analysis. The following corrections have been made:

1. Section 2 (Methods):

- The revised text now includes specific details of the experimental setup: manufacturer and model of the HUBER X-ray diffraction system, goniometer configuration, collimator aperture, scan parameters, and data acquisition software (SPEC Control Software).

- Additional details have been added on repeated measurements (triplicate readings), calculation of mean values, standard deviations, and propagation of error for wavelength and energy estimations.

- Statistical reliability criteria (<2% relative uncertainty) have been introduced to validate the results.

2. Minor textual clarifications were made to improve reproducibility and accuracy of the described procedure.

Additionally, the following references have been updated:

– "Fitted empirical reference cross sections for K-shell ionization by protons / H. Paul, J. Sacher // Atomic Data and Nuclear Data Tables. — 1989. — Vol. 42, No. 1. — P. 105–156" has been replaced with "Empirical K-shell ionization cross-sections of elements from 4Be to 92U by proton impact / A. Kahoul, M. Nekkab, B. Deghfel // Nuclear Instruments and Methods in Physics Research, Section B: Beam Interactions with Materials and Atoms. — 2008. — Vol. 266, No. 23. — P. 4969–4975. https://doi.org/10.1016/j.nimb.2008.09.008";

– "Cross Sections for K-shell X-ray Production by Hydrogen and Helium Ions in Elements from Beryllium to Uranium / G. Lapicki // Journal of Physical and Chemical Reference Data. — 1989. — Vol. 18, No. 1. — P. 111–218. https://doi.org/10.1063/1.555838" have been replaced with "Feasibility study of thin films deposited on a self-supporting carbon grid substrate target on the measurement of atomic inner-shell ionization cross-sections impacted by 3-30 keV electrons / Z. C. Qian, Y. Wu, C. H. Chang, Y. Yuan, C. S. Mei, J. J. Zhu, K. Moharram // EPL. — 2017. — Vol. 118, No. 1. — Article number. 13001. https://doi.org/10.1209/0295-5075/118/13001";

– "Energy-loss effect in inner-shell Coulomb ionization by heavy charged particles / W. Brandt, G. Lapicki // Physical Review A. — 1981. — Vol. 23, No. 4. — P. 1717–1729" have been replaced with "Theoretical models to calculate stopping and ionization ratios of H2+ molecules in solid targets / C. D. Archubi, N. R. N. Arista // Physical Review A. — 2019. — Vol. 99, No. 3. — Article number 032702. https://doi.org/10.1103/PhysRevA.99.032702";

– "Specific conductance of the molten LiF-KCl and LiF-KBr systems / C. Xu, G. Liu, N. Chen // Jinshu Xuebao/Acta Metallurgica Sinica. — 1984. — Vol. 20, No. 5. — P. b320–b322." Have been replaced with "Phase Assemblage of the Li+,Na+,K+||F–,Cl–,Br– Five-Component Reciprocal

System and Its LiF–KCl–KBr–NaBr–NaCl Stable Pentatope / A.V. Burchakov, I. K. Garkushin, U. A. Emel'yanova Russian Journal of Inorganic Chemistry. — 2023. — Vol. 68, No. 7. — P.889–897. https://doi.org/10.1134/S003602362360082X".

These amendments do not affect the scientific results, discussion, or conclusions of the paper but enhance methodological transparency.

Published: 20.03.2024